Pergamon

Bioorganic & Medicinal Chemistry, Vol. 4, No. 10, pp 1715–1724, 1996

PII: S0968-0896(96)00184-8
0968-0896/96 $15.00+0.00

Investigation on QSAR and Binding Mode of a New Class of Human Rhinovirus-14 Inhibitors by CoMFA and Docking Experiments

Marino Artico,[a] Maurizio Botta,[b,c,*] Federico Corelli,[b,c,*] Antonello Mai,[a] Silvio Massa[b] and Rino Ragno[b,†]

[a]*Dipartimento di Studi Farmaceutici, Università 'La Sapienza', P.le A. Moro 5, I-00185 Roma, Italy*
[b]*Dipartimento Farmaco Chimico Tecnologico*
[c]*Centro Interdipartimentale per lo Studio Strutturale dei Sistemi Biomolecolari, Università di Siena, Banchi di Sotto 55, I-53100 Siena, Italy*

Abstract—A 3-D QSAR study has been carried out on a new class of potent and selective human rhinovirus-14 (HRV-14) inhibitors. In particular, the CoMFA (comparative molecular field analysis) technique has been applied to develop a model able to explain and predict the anti-HRV-14 activity of a class of compounds **4** and potentially helpful to design new and more potent antirhinovirus agents. Docking experiments have also been performed with the aim of elucidating the possible binding mode of these inhibitors. These two approaches are combined to highlight a single, highly favoured mode of interaction of the compounds with the viral capsid proteins. Copyright © 1996 Elsevier Science Ltd

Introduction

A vast group of diseases threatening both humans and animals can be attributed etiologically to different members of the picornavirus family. This is a large family of viral pathogens that are phylogenetically subdivided according to their buoyant density, pH stability, and sedimentation coefficients into the following four genera: (1) enterovirus, which includes polio, hepatitis A, and coxsackie viruses; (2) cardiovirus, which includes the encephalomyocarditis and mengo viruses; (3) apthovirus, which includes the foot-and-mouth disease virus, or FMDV; and (4) rhinoviruses, which are responsible for approximately 40% of the common cold and mild localized infections of the upper respiratory tract in humans.

Peculiar to the picornaviruses, and in particular to rhinoviruses, is their remarkable heterogeneity (human rhinovirus, or HRV, has no less than 89 and probably more than 100 serotypes[1]), which has hampered the development of vaccines and made troublesome the design of effective, broad-spectrum drugs.

During the last decade, Diana's group at the Sterling Winthrop Research Institute has contributed important information on the design of antirhinovirus agents.[2–10] Beginning with arildone (**1**) (Chart 1) and followed by disoxaril (**2a**, $n=7$, $R=R_1=H$), WIN 54954 (**3**), and their analogues, generally defined [(oxazolylphenoxy)alkyl]isoxazoles, an increasingly better activity, in terms of potency and spectrum of action, against rhinoviruses and other picornaviruses was reported.[2,3] None of these antipicornaviral agents has overcome clinical studies either because of undesired side-effects, such as crystalluria (disoxaril), or unfavourable pharmacokinetics (WIN 54954).[4] X-Ray crystallographic studies of drug-human rhinovirion complexes have shown that disoxaril and its analogues bind in a hydrophobic pocket beneath the canyon floor and either block the uncoating process by stabilizing the virion structure or lead to conformational changes which affect the putative viral receptor binding site, thus preventing virion adsorption to cell receptors.[5–7] Molecular dynamics simulation techniques using methods of ligand-based and high-temperature conformational searching have also been exploited to investigate disoxaril-VP1 interactions.[11] In order to develop SAR around [(oxazolylphenoxy)alkyl]isoxazoles, the effects of substitution on the phenyl ring,[8] variation of the connecting chain length,[9] and heterocyclic replacements of the oxazoline ring[10] have been investigated by Diana and coworkers.

In the course of our studies[12–16] directed toward the identification of agents useful in the prophylaxis and therapy of HRV infections, we decided to perform more extensive structural modifications of [(oxazolylphenoxy)alkyl]isoxazoles, exploring the question of whether the isoxazole nucleus plays a fundamental role in the interaction of these compounds with the amino acids of the viral capsid protein 1 (VP1) or could be replaced by isosteric rings. Accordingly, we reported the synthesis of new compounds **4** and **5** (Chart 1), characterized by pentatomic heterocycles different

†On leave from Dipartimento di Studi di Chimica e Tecnologia delle Sostanze Biologicamente Attive, Università 'La Sapienza', P.le A. Moro 5, I-00185 Roma, Italy.

from isoxazole and by the presence of a carbonyl group in the aliphatic chain. Congeners **6**, without carbonyl group in the chain, as well as benzene analogues **4i,q** were also prepared and tested for antiviral activity.

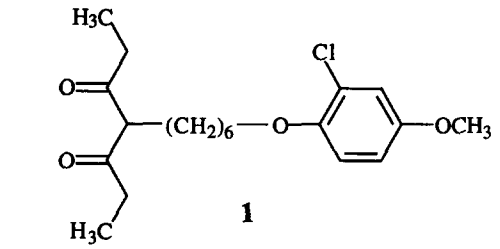

1

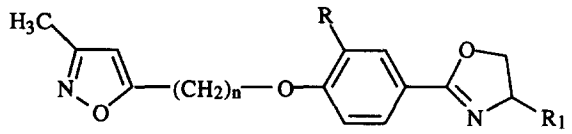

2a-g

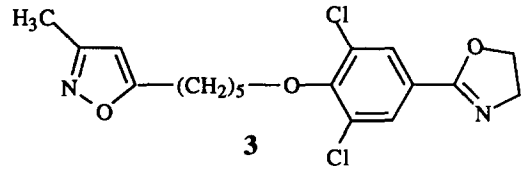

3

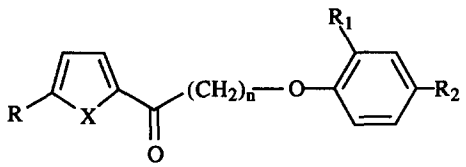

4a-q X = S, O, NCH_3, CH=CH
n = 4, 6
R = H, Cl, CH_3
R_1 = H, Cl
R_2 = $CO_2C_2H_5$, 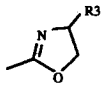
R_3 = H, (*R* or *S*)-CH_3

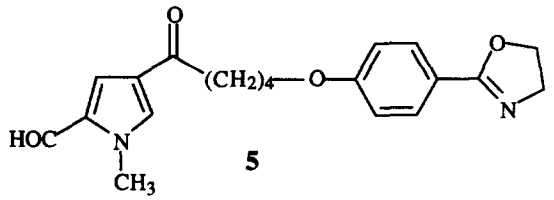

5

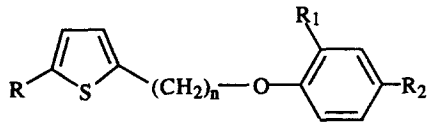

6a-e n = 5, 7
R = Cl, CH_3
R_1 = H, Cl
R_2 = $CO_2C_2H_5$, 

Chart 1. Structures of the compounds considered in this study. See also Tables 1, 2, and 4.

Some thiophene, pyrrole, and furan derivatives showed potent and selective activity against HRV-14. It is worth pointing out that contrary to disoxaril, which is cytotoxic at a concentration of 36.7 μM, most of compounds **4** are far less toxic and in some cases exhibit more than a 10-fold more favourable selectivity index (SI), defined as the ratio between CC_{50} (compound concentration required to reduce the viability of mock-infected HeLa cells by 50%) and MIC_{80} (compound concentration that inhibits 80% of the serotypes tested). The structural feature that seems to ensure the best biological profile, in terms of both anti-HRV-14 activity and cytotoxicity, is the carbonyl group that definitely differentiates this class of antirhinoviral agents from [(oxazolylphenoxy)alkyl]isoxazoles. With the aim of establishing the actual role of this structural component and hence its influence on the anti-HRV-14 activity, we have undertaken a 3-D QSAR study. In particular, the CoMFA (comparative molecular field analysis) technique has been applied to develop a model able to explain and predict the anti-HRV-14 activity of compounds of general structure **4** and is helpful in designing new and more potent antirhinovirus agents.

Methods

CoMFA is a three-dimensional approach to quantitative structure–activity correlation.[17] It attempts to correlate receptor–ligand affinities with the steric and electrostatic fields presented by the substrates, thus describing both the electronics and shape. Steric and electrostatic fields of a given set of molecules are sampled at the interactions of a three-dimensional lattice in which they are aligned. Once a suitable alignment has been achieved, independent steric and electrostatic regressor values are generated at each lattice point. These calculated values together with the dependent variable are included in a partial least squares (PLS) analysis utilizing cross-validation for the development of a model with predictive utility for the 'activities' of untested molecules. The cross-validation technique involves random elimination of one or more observations from the original data set with subsequent equation development and activity prediction for the eliminated observation in an iterative manner, thus yielding a QSAR equation that is generally of greater predictive value than that derived from conventional regression analysis. Correlations yielding a cross-validated $q^2 \geq 0.50$ are considered to be of predictive utility. Finally, graphic representation of the results is given.

In addition to the steric and electrostatic parameters, we have considered in our analysis also the chromatographic capacity factor (k') that has often been used as a hydrophobic index of bioactive compounds. The capacity factor k' is defined by eq (1), where t_R is the retention time of the compound and t_0 is the column dead time.

$$k' = (t_R/t_0 - 1). \quad (1)$$

Generally, there exists a linear relationship between the logarithm of the capacity factor (log k') and the octanol-water partition coefficient (log P) determined by the standard shake-flask method.[18]

Compound selection

Tables 1 and 2 list the structures and the observed and calculated biological activity values of compounds **4a–l**, **5**, and **6a–d**, forming the training set used to derive the CoMFA model, and of compounds **4m–q** and **6e** forming the set used to test the predictivity of the model itself.

The compounds were screened[14–16] in a tetrazolium-based colorimetric assay (MTT assay) using HeLa-Ohio cells and their anti-HRV-14 activity was evaluated by means of EC_{50} defined as the compound concentration (μM) required to achieve 50% protection of HeLa cells from HRV-14 induced cytopathic effect. In this CoMFA study, the biological activity of each compound has been expressed as pEC_{50}. Consequently, all the activity values are in the range of −1.06 (less active compound) to +0.89 (more active compound). Compounds forming the training and test sets were chosen so as to cover all the activity range, from the less to the more potent compound, in order to ensure the uniform sampling of the biological

Table 1. Observed and calculated in vitro anti-HRV-14 activity values of the compounds forming the training set

Compound	R	R_1	R_2	X	*n*	log k'	pEC_{50}[a]		
							obsd[b]	calcd[c]	res[d]
4a	Cl	H	COOEt	S	4	0.721	0.27	0.44	−0.17
4b	Cl	H	OX[e]	S	4	0.628	0.89	0.82	0.07
4c	H	H	OX[e]	N—CH_3	4	0.803	−0.29	−0.27	−0.02
4d	CH_3	H	COOEt	S	4	0.591	−0.57	−0.55	−0.02
4e	CH_3	H	OX[e]	S	4	0.477	0.54	0.49	0.05
4f	CH_3	Cl	OX[e]	S	4	0.644	0.85	0.84	0.01
4g	CH_3	H	DMOX[f]	S	4	0.604	−0.22	−0.34	0.12
4h	CH_3	H	DMOX[f]	S	6	0.911	0.09	−0.04	0.13
4i	CH_3	H	COOEt	CH=CH	4	0.580	0.57	0.45	0.12
4j	CH_3	H	(*R*)-MOX[g]	S	4	0.542	−0.75	−0.77	0.02
4k	CH_3	H	(*S*)-MOX[h]	S	6	0.843	−0.29	−0.12	−0.17
4l	CH_3	H	(*R*)-MOX[g]	S	6	0.848	0.58	0.65	−0.07
5	CHO	H	OX[e]	N—CH_3	4	0.149	−0.19	−0.07	−0.12
6a	Cl	H	OX[e]	S	5	1.289	−0.46	−0.44	−0.02
6b	CH_3	H	OX[e]	S	5	1.297	−1.06	−1.09	0.03
6c	CH_3	H	COOEt	S	5	1.338	−0.86	−0.81	−0.05
6d	CH_3	Cl	OX[e]	S	7	0.950	−0.12	−0.18	0.06

[a]$pEC_{50} = \log(1/EC_{50})$, where EC_{50} is the compound concentration (μM) required to achieve 50% protection of HeLa cells from HRV-14 induced cytopathic effect.
[b]Experimental data taken from refs 14–16.
[c]Values calculated according to the calibration model I.
[d]Difference between observed and calculated values.
[e]OX = 4,5-dihydrooxazol-2-yl.
[f]DMOX = 4,5-dihydro-5,5-dimethyloxazol-2-yl.
[g](*R*)-MOX = (*R*)-4,5-dihydro-5-methyloxazol-2-yl.
[h](*S*)-MOX = (*S*)-4,5-dihydro-5-methyloxazol-2-yl.

Table 2. Observed and predicted in vitro anti-HRV-14 activity values of the compounds forming the test set

Compound	R	R_1	R_2	X	*n*	log k'	pEC_{50}[a]		
							obsd[b]	pred[c]	res[d]
4m	CH_3	H	COOEt	O	4	0.364	−0.38	0.51	0.13
4n	CH_3	H	OX[e]	S	6	0.775	−0.11	0.00	−0.11
4o	CH_3	H	(*S*)-MOX[f]	S	4	0.520	0.55	−0.19	0.74
4p	CH_3	H	COOEt	S	6	0.869	−0.26	0.47	−0.73
4q	H	H	COOEt	CH=CH	4	0.485	−1.05	−0.59	−0.46
6e	Cl	H	COOEt	S	5	1.375	−0.96	−1.21	0.25

[a,b,e]See the corresponding footnotes of Table 1.
[c]Values predicted according to the non-cross-validated model I.
[d]Difference between observed and predicted values.
[f]See footnote h of Table 1.

activity. Compounds were not added or removed from these sets for obtaining higher correlation coefficients.

Molecular modeling and alignment rules

Due to the lack of X-ray crystallographic information about compounds forming the training and the test sets, their input geometries were generated and initially minimized by using the program MODEL (version KS 2.99).[19] In order to evaluate the putative global minimum energy conformations of our compounds, a conformational analysis was carried out using the modified MM2 force field as implemented in the program BKMDL.[19] We chose the STATISTICAL method of conformational search since it is less computationally demanding than the GRID method when dealing with such flexible molecules as those considered. sp^2–sp^2, sp^2–sp^3, and sp^3–sp^3 bonds were rotated by increments of 180, 30, and 120°, respectively. The search was stopped when duplicate geometries were mostly generated and the global minimum structure had been found several times. Following this procedure a set of conformers within 3 kcal/mol from the global minimum energy conformer was generated for each of the compounds **1a–w**.

The resulting minimum energy and most of the conformers showed a U-shaped geometry probably due to the hydrophobic collapsing between the two aromatic rings. However, extended geometries were also present in each set of conformers.

Since CoMFA is a shape-dependent technique,[20] its calculated field values are highly dependent on the conformation of the considered molecules and their relative orientations. Considering the lack of X-ray crystallographic data on the studied compounds and their structural similarity to disoxaril and its analogues, we resorted to the crystallographic data of the complexes between HRV-14 and **2a** and **b** ($n=5$, $R=R_1=H$) available from the Brookhaven Protein Data Bank (PDB). Thus, the coordinates of **2a** and **b** were extracted from the crystal structure of their complexes and used to build molecules having seven and five carbon atoms in the chain, respectively, by using the MODIFY option in Sybyl (version 6.0).[21] Structures were then optimized using the standard Tripos force field with 0.001 kcal/mol energy gradient convergence criterion and distance-dependent dielectric term.

The 'alignment rule', that is the superimposition of the molecular models within a three-dimensional fixed lattice, is one of the most important input variables in CoMFA. For this purpose, flexible compounds are by far the most difficult to model. To define the alignment rules for a flexible training set, one can use a variety of methods that are generally dependent on whether or not crystallographic data are available. In our case, since the binding mode of disoxaril and related analogues to VP1 has been already described, molecules were aligned to **2b** using the FIT option in Sybyl (atom by atom) choosing all of the non volatile atoms.

One of the variables in the CoMFA procedure is the calculation of the point charges. However, from recent publications there is strong evidence to suggest that in CoMFA the overall influence of the point charges is not sensitive to the method how these are calculated.[22] Therefore, the partial atomic charges for all the molecules were computed with Sybyl using the GASTHUCK method of this program and were used without further refinement.

3D-QSAR methodology

CoMFA calculations were performed using the QSAR module of Sybyl and with the following characteristics: the grid in which the molecules were embedded was regularly spaced (2 Å) in each direction with the grid extending 4.0 Å in every direction away from the molecule. The CoMFA lattice was $25.75 \times 24.69 \times 17.81$ Å ($x=-12.12$ to 13.63, $y=-13.79$ to 10.90, $z=-8.91$ to 8.60) with 1521 points. Steric and electrostatic interaction energies were calculated using an sp^3 carbon probe atom with a van der Waals radius of 1.52 Å and +1 charge, a distance-dependent dielectric function ($1/r$), and an energetic cut off of ± 30 kcal/mol. The electrostatic energy term was ignored at lattice intersections yielding maximal (± 30 kcal/mol) steric values. The same three-dimesional grid was used in all the CoMFA studies.

Regression analyses were done using the Partial Least Squares (PLS)[23] with Principal Component Analysis (PCA)[24] algorithms as implemented in Sybyl, initially with cross-validation (the leave-one-out technique) to reduce the probability of obtaining chance correlations and five principal components (PCs).[25,26] The number of groups of cross-validation was set equal to the number of components of the training set. To improve the signal-to-noise ratio, all leave-one-out calculations were performed selecting a 2.0 kcal/mol energy column filter (the so called minimum_sigma option or field variance at each grid point was used for this purpose). The steric and electrostatic field columns were weighted according to the COMFA_STD default scaling option. In this method a field is considered as a whole and every CoMFA variable is affected by the overall field mean and standard deviation. Final PLS (non cross-validated models) calibration equations were then derived using the optimal number of components so identified.

To assist selection among various 3-D QSAR calibration equations (models) and to test their utility as predictive tools, an external set (the so called test set) of compounds with known activities not used in model generation was predicted. The predictive r^2 based only on molecules from the test set is normally reported as the most appropriate parameter to evaluate the predictive power of a CoMFA model. Predictive r^2 is calculated using the following equation:

predictive $r^2 = 1 - (\text{'press'}/\text{SD})$,

where SD is the sum of the squared deviations between the actual activities of the compounds in the test set and the mean activity of the training set compounds and 'press' is the sum of the squared deviations between predicted and actual activities for every compound in the test set. It is obvious from the equation that prediction of the mean value of the training set for every member in the test set yields a predictive $r^2=0$, while negative values are possible when the predictions are worse than predicting the mean value of the training set. This procedure was followed to evaluate the predictive ability of our CoMFA models.

As a further attempt to validate the best CoMFA model obtained, the bootstrap validation method[25] was used as implemented in Sybyl. This technique is used to estimate the stability of the parameters (mean and standard deviation) associated with the statistical models.

CoMFA coefficients contour maps of the coefficients of each grid point were also generated by following the standard procedure in Sybyl. These maps show lattice points where the QSAR strongly associates changes in steric and electrostatic field values with changes in biological activity in order to obtain chemical information.

Results and Discussion

The initial cross-validated analysis using the 17 compounds in the training set and considering only steric and electrostatic parameters identified five optimal components with a cross-validated q^2 value of 0.72 and a SEP of 0.38 log units. The corresponding non-cross-validated analysis (5 components) resulted in a conventional correlation coefficient (r^2_{corr}) value of 0.98 with a standard error of estimate (SEE) of 0.11 log units (F-test value equal to 87.14). The contributions of steric and electrostatic fields to the QSAR equation were 62.5 and 37.5%, respectively (Model I, Table 3). When the lipophilicity parameters log k' and log k'^2 were also considered in the 3D QSAR analysis, a second, only slightly more significant model ($q^2=0.76$; SEP=0.34; $r^2_{corr}=0.94$; SEE=0.11; F-test=48.68) was obtained (Model II, Table 3). In this second case, the optimal number of components found was equal to 4 and the contributions of steric field, electrostatic field, log k' and log k'^2 are, respectively, 54, 22, 25, and 1%. Since the two models exhibit substantially the same statistical significance, the first one (model I) was chosen because it does not require the knowledge of log k' and hence could be applied to either not yet synthesized or known molecules, whose lipophilicity parameters are not available. A high bootstrapped q^2 value of 0.97 ± 0.02 with a correspondingly small SEE (0.12 ± 0.09 log units) adds a high degree of confidence to this analysis. Figure 1 depicts a plot of observed vs calculated in vitro anti-HRV-14 activities of compounds **4a–l**, **5**, and **6a–d** (training set) using the optimal non-cross-validated model I.

Table 3. Statistics of the calibration CoMFA models

Regressors	Model I CoMFA (S, E)	Model II CoMFA (S, E), log k', log k'^2
r^2_{corr}	0.97	0.94
SEE	0.11	0.17
F-test	87.14	48.68
q^2_{cv}	0.72	0.76
SEP	0.38	0.34
no. of components	5	4
% of contribution	62.5, 37.5	54, 22, 25, 1
Average absolute error of prediction	0.53	0.58

Evaluation of the predictive power of this CoMFA model using the six compounds **4m–q** and **6e** (test set) resulted in a r^2_{pred} of 0.56. From Table 2, it can be seen that the activities of all the examined compounds are predicted within 0.74 log units of their actual pEC_{50} with an average absolute error of 0.58 log units across a range of 1.6 log units. The predictive power results are shown in Figure 1, which reports a plot of measured vs predicted pEC_{50} using the non-cross-validated model I.

The CoMFA steric and electrostatic fields for this analysis are shown as contour maps in Figures 2 and 3. The field values were calculated at each grid point as the scalar product of the associated QSAR coefficient and the standard deviation of all values in the corresponding column of the data table (STDEV*COEFF), and always plotted as the percentage of contribution to the QSAR equation. These surfaces are to be

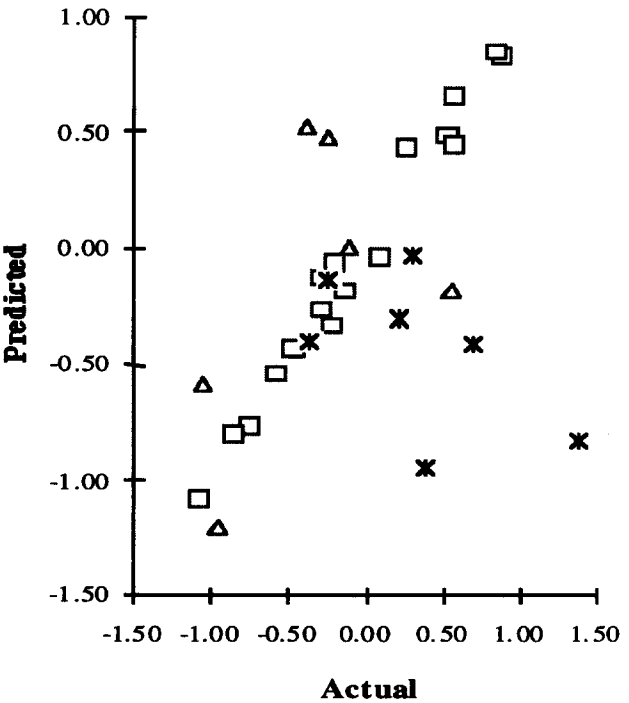

Figure 1. Predicted (calculated) vs actual values of pEC_{50}. □ Compounds of the training set, △ compounds of the test set; * **2a–g**.

considered as a representation of the lattice points, where differences in field values are strongly associated with differences in inhibitory potency. Though the interpretation of these maps is primarily intuitive and highly subjective, the absence of the lattice points does not mean that a given pharmacophore element has no influence on the biological activity. It can also indicate that all the examined compounds exert the same steric/electrostatic influence in a certain area or, as suggested by Cramer et al.,[20] can help to delineate the less explored volume of a lattice.

In Figure 2, areas of high steric bulk tolerance (80% contribution), represented by green polyhedra, are noted in the vicinity of the carbonyl group and above the dihydrooxazolyl or ethoxycarbonyl moiety. This part of the molecular structure is almost the same in all the compounds of the training set, with the exception of those lacking the carbonyl in the chain that are the less active compounds. Areas of low steric bulk tolerance (20% contribution) represented by yellow polyhedra are principally located near the heteroaromatic ring and below the dihydrooxazoline moiety.

Figure 2. CoMFA steric STDEV*COEFF contour plot from the analysis based on model I. Sterically favoured areas (80% contribution level) are represented by green polyhedra. Sterically disfavoured areas (20% contribution level) are represented by yellow polyhedra. All the compounds forming the training set are represented.

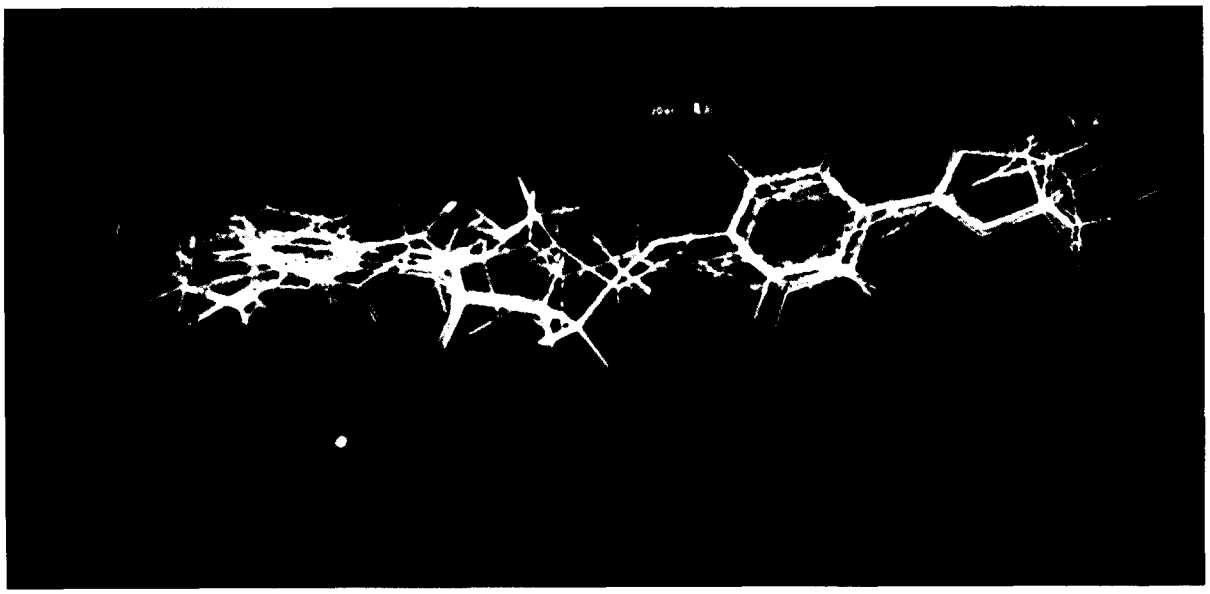

Figure 3. CoMFA electrostatic STDEV*COEFF contour plot from the analysis based on model I. Negative charge favoured areas (80% contribution level) are represented by blue polyhedra. Negative charge disfavoured areas (20% contribution level) are represented by red polyhedra. All the compounds forming the training set are represented.

In Figure 3 (electrostatic contour maps), areas of increased tolerance for negative charge (80% contribution), designated by the blue polyhedra, are present above and below the plane of the heteroaromatic ring, while areas of decreased tolerance for negative charge (20% contribution), represented by red polyhedra, are located in proximity of the substituent of the heteroaromatic nucleus as well as near the carbonyl and the oxygen atom in the chain.

From the results reported above, a good correlation can be noted between the antiviral activity of compounds **4–6** and their physicochemical properties, the most important of which seems to be the steric hindrance, which is related to more than 60% of the explained variance. However, no conclusive explanation of the positive influence of the carbonyl group on the biological activity can be given.

Our CoMFA model was subsequently tested on Diana's compounds **2a–g**. As can be seen in Table 4 and Figure 1, the model was able to predict the activity of compounds **2a–d** within 0.53 log units of their actual pEC_{50}, whereas compounds **2e–g** were mispredicted. It is interesting to note that **2a–d** bind into the virus pocket by locating the dihydrooxazolinyl moiety and the isoxazole ring into the 'toe' and the 'heel', respectively, of the foot-shaped cavity of the virus (disoxaril-like orientation); on the contrary, compounds **2e–g** are known to assume the opposite orientation. On the basis of our results, we hypothesize that all the compounds **4–6** enter into the virus in a disoxaril-like orientation and such a hypothesis is supported by the following observations.

1. Compounds **2e–g**, with methyl group(s) on the dihydrooxazole ring, show enhanced activity with respect to the unsubstituted derivative **2a**. Furthermore, the activity of **2e,f** is crucially dependent on the absolute stereochemistry of the chiral center on the dihydrooxazole ring. This has been explained on the basis of hydrophobic interactions of (*S*)-enantiomers with Leu^{106} and Ser^{107}, which in turn, favourably orient the nitrogen of the oxazoline ring to hydrogen bond with Asn^{219}.[28] As a result, (*S*)-isomers display greater levels of activity than the *R*.

Table 4. Observed and predicted in vitro anti-HRV-14 activity values of the compounds **2a–g**

Compound	R	R_1	*n*	pEC_{50}[a]		
				obsd[b]	pred[c]	res[d]
2a	H	H	7	−0.25	−0.13	−0.12
2b	H	H	5	0.30	−0.03	0.33
2c	Cl	H	5	−0.38	−0.41	0.03
2d	H	(*S*)-CH_3	5	0.22	−0.31	0.53
2e	H	(*R*)-CH_3	7	0.40	−0.95	1.35
2f	H	(*S*)-CH_3	7	1.40	−0.84	2.24
2g	Cl	(*R,S*)-CH_3	7	0.70	−0.41	1.11

[a,c,d]See the corresponding footnotes of Table 2.
[b]Data taken from ref. 27.

2. Neither compounds **2a–d** (known to bind in a disoxaril-like orientation) nor compounds **4–6** show such a marked enantiomeric effect. Moreover, even the presence of methyl group(s) on the oxazoline ring seems not to affect the antiviral activity in a definite way.
3. The electrostatic potential of compound **2**, displayed by isocontour surfaces, shows approximately a symmetrical pattern with respect to the long axis of the molecule, thus allowing these compounds to bind into the virus pocket either in the disoxaril-like orientation or in the opposite one, depending upon their structural features (basically, the chain length and the presence of substituent on the oxazoline ring). From the comparison of the electrostatic potential surface of **4e** (representative example of the new family of compounds) with those of **2a**, **2b**, and **2f** (Fig. 4), it results that compound **4e** lacks any symmetry, most likely as a consequence of the presence of the carbonyl group. It might be possible that this structural moiety act as a further constraint in order for compounds **4** to assume a disoxaril-like orientation inside the virus.

Our hypothesis on the mode of binding of derivatives **4–6** to VP1 is further confirmed by docking experiments performed with Sybyl on **4b** and VP1 according to the following procedure. The coordinates of **2b** were extracted from the crystal structure of its complex with HRV-14, thus creating the cavity where **4b** (for geometry optimization of **4b** and its alignment to **2b**, see Molecular modeling and alignment rules) could be fitted. All the amino acid residues of the capsid proteins more than 10 Å distant from each atom of the ligand were cut to reduce the computing demand, this being justified by the fact that steric and electrostatic interactions at a distance >10 Å have little, if any, influence on the whole ligand–protein interaction. Molecules of crystallization water were also not considered. Assuming that the dihydrooxazoline moiety is already quite well positioned inside the pocket (same orientation as in the reference compound **2b**), only the dihedral angles 1–2–3–4 and 4–3–5–6 (Table 5) were varied during the docking experiments, while the amino acid residues of the cavity were kept fixed. Abatement of small van der Waals interactions occurring between the ligand and the protein during the docking experiments via molecular mechanics calculations led to the *computationally co-crystallized complexes*[29] of **4b** with VP1 (complexes 1–4 in Table 5). With the aim of exhaustively investigating the possible role of the carbonyl group in dictating the orientation of **4b** into the virus pocket, also complexes 5–8, where the ligand has been docked in the opposite orientation (disoxaril-unlike), were similarly built up.

Diana and co-workers reported that the interactions between [(oxazolylphenoxy)alkyl]isoxazoles and the virus are almost entirely hydrophobic, although a hydrogen bond has been found between Asn^{219} of the viral protein and the isoxazole or the oxazoline ring of the ligand, depending on the disposal of the specific compound into the virus.[27] Nevertheless, by inspection

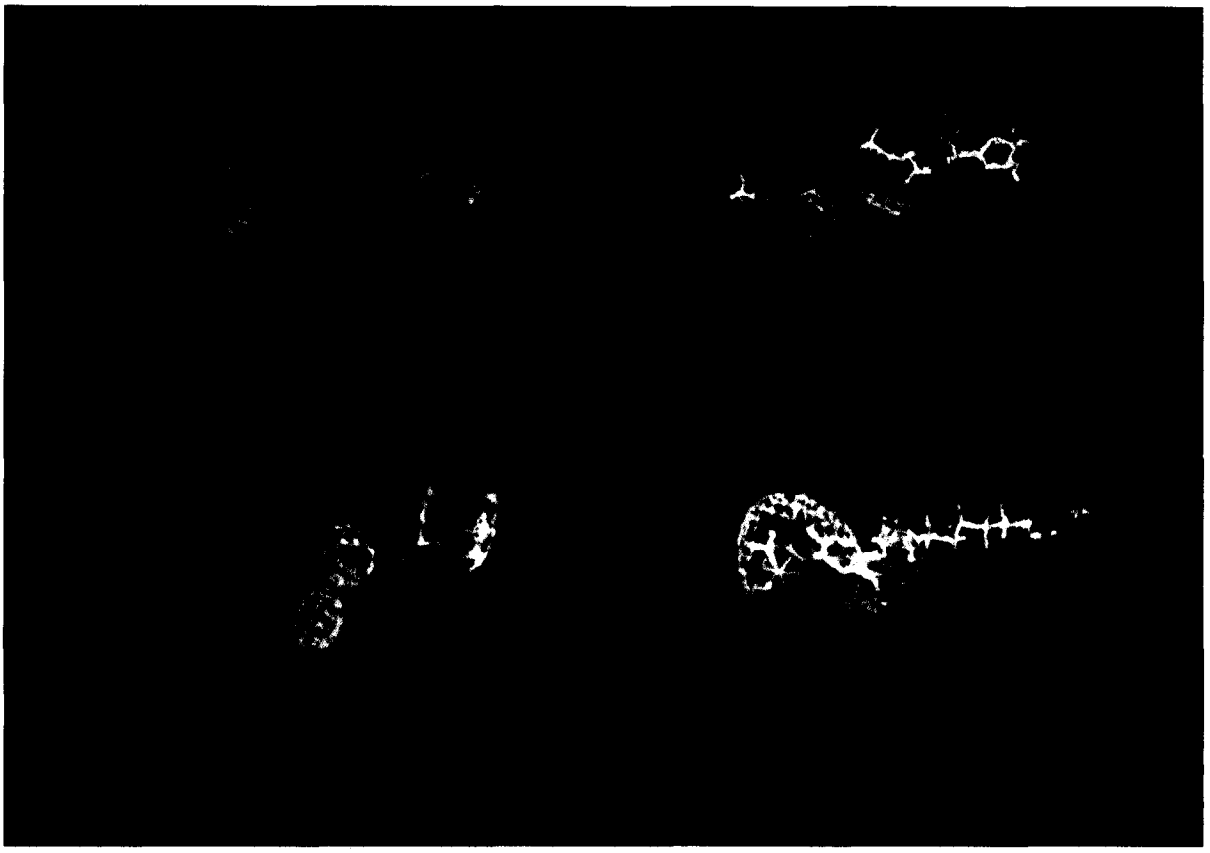

Figure 4. Electrostatic potenials calculated from Gasteiger–Hückel charges (blue: 1 kcal/mol; red: −1 kcal/mol) are displayed by isocontour surfaces. Compounds **2a** (left-upper), **2b** (right-upper), and **2f** (right-lower) possess approximately a symmetrical pattern with respect to the long axis of the molecule, whereas compound **4e** (left-lower) shows an unsymmetrical distribution of the electrostatic potential.

Table 5. Characteristics of the complexes between VP1 and **4b** obtained by docking experiments

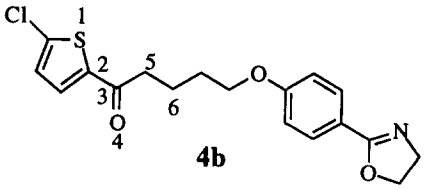

4b

Complex	Dihedral angle 1–2–3–4	Dihedral angle 4–3–5–6	Orientation of the ligand[a]	Interaction energy (kcal/mol)		
				E_{electr}	E_{steric}	E_{total}
1	0	0	DL	−3.765	−37.510	−41.275
2	0	180	DL	2.313	−40.318	−38.005
3	180	180	DL	0.162	−40.919	−40.757
4	180	0	DL	−8.062	−33.045	−41.107
5	0	0	DU	2.424	−28.660	−26.236
6	0	180	DU	−1.281	−23.308	−24.589
7	180	180	DU	−1.715	−26.900	−28.615
8	180	0	DU	1.078	−36.335	−35.257
9 (1 + H_2O)	0	0	DL	−3.135	−38.884	−42.019

[a]DL = disoxaril-like; DU = disoxaril-unlike.

of the complexes obtained from the Brookhaven PDB, we noticed that such a hydrogen bond involves an intermediate molecule of water. Compound **4b** in complexes 1–4 shows the carbonyl group oriented toward Asn^{219} but too far from it to act as a H-bond acceptor (Fig. 5). On the other hand, when a water molecule was placed between the carbonyl oxygen of our ligand and Asn^{219}, the program Sybyl actually recognized the possibility of hydrogen bond, that could further stabilize the complex (approximately 1 kcal/mol).

As seen in Table 5, complexes 1–4 are more stable than complexes 5–8, the energy difference between complexes varying only for the relative orientation of the ligand (1–5, 2–6, 3–7, and 4–8) being in the range of 6–15 kcal/mol.[30]

In the light of these findings, we feel that the carbonyl of compounds **4,5** does not play the major role of H-bond acceptor group, though such a possibility cannot definitely ruled out, but rather it strongly concurs with the other structural characteristics of this new class of HRV-14 inhibitors to determine a single, highly favoured mode of binding to the viral capsid proteins.

Experimental

Determination of the chromatographic capacity factor k'

The lipophilicity of the compounds was determined by HPLC using a Waters system with a Knauer variable wavelength monitor operating at 214 nm, a Merck RP18 5 μm LiChrosorb (4 × 250 mm) column. Peak registration and retention times were obtained with a Pharmacia LKB-REC2 registrator. *n*-Decylamine (0.2%, v/v) was used as a masking agent to eliminate silanophilic interactions.[31] Capacity factors, log k', were experimentally determined using methanol–phosphate buffer (ammonium phosphate pH 7.4, 0.05 M) mixture as eluent at a flow of 2 mL/min. Generally, 10 μL of each sample as a solution in methanol (1 mg/mL) were injected. The column dead time was determined by the peak of the methanol used for the preparation of the solutions. Attempts to obtain the log k'_w were not effective because of the high retention time of the compounds at higher percentage of buffer.

Molecular modeling and docking experiments

Molecular mechanics calculations were performed with use of the program MODEL (version KS 2.99)[19] on a Digital VAXSTATION II/GPX computer and Sybyl program[21] on a Silicon Graphics 4D/35 Personal Iris.

The input structures of the ligand–receptor complexes were obtained by docking the ligand in the X-ray structure of the receptor. The complexes were energy-minimized according to the default options of Sybyl. In order to optimize interactions, minimizations were repeated several times, with different initial orientations of the ligand with respect to the receptor amino acid residues, which were kept fixed. Point charges of the ligand were computed using the GAST–HUCK method, while Pullmann charges were used for the protein receptor.

Acknowledgments

The authors from Siena are grateful to the Italian CNR (Comitato Nazionale Biotecnologie e Biologia Molecolare) for financial support of this work. The authors from Rome gratefully acknowledge support from Italian MURST, 60% funds (Progetti Ateneo, Università di Roma).

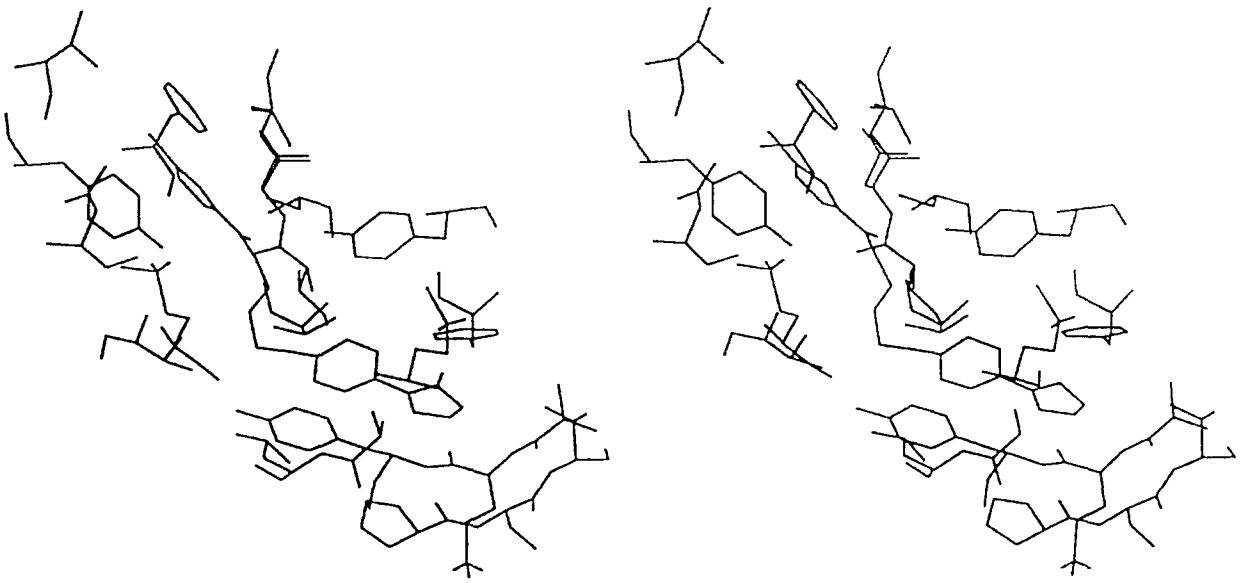

Figure 5. Result of docking experiments of **4b** into the binding site of HRV-14 (stereoview).

References and Notes

1. Hamparian, V. V.; Colonno, R. J.; Cooney, M. K.; Dick, E. K.; Gwaltney, J. M.; Hughes, J. H.; Jordan, W. S.; Kapikian, A. Z.; Mogabgab, W. J.; Monto, A.; Phillips, C. A.; Reuckert, R. R.; Schieble, J. H.; Stott, E. J.; Tyrrell, D. A. J. *Virology* **1987**, *159*, 191.

2. Diana, G. D.; Cutcliffe, D.; Oglesby, R. C.; Otto, M. J.; Mallamo, J. P.; Akullian, V.; McKinlay, M. A. *J. Med. Chem.* **1989**, *32*, 450.

3. Woods, M. G.; Diana, G. D.; Rogge, M. C.; Otto, M. J.; Dutko, F. J.; McKinlay, M. A. *Antimicrob. Agents Chemother.* **1989**, *33*, 2069.

4. Diana, G. D.; Volkots, D. L.; Nitz, T. J.; Bailey, T. R.; Long, M. A.; Vescio, N.; Aldous, S.; Pevear, D. C.; Dutko, F. J. *J. Med. Chem.* **1994**, *37*, 2421.

5. Fox, M. P.; Otto, M. J.; McKinlay, M. A. *Antimicrob. Agents Chemother.* **1986**, *30*, 110.

6. Pevear, D. C.; Fancher, M. J.; Felock, P. J.; Rossmann, M. G.; Miller, M. S.; Diana, G. D.; Treasurywala, A. M.; McKinlay, M. A.; Dutko, F. J. *J. Virol.* **1989**, *63*, 2002.

7. Smith, T. J.; Kremer, M. J.; Luo, M.; Vriend, G.; Arnold, E.; Kamer, G.; Rossmann, M. G.; McKinlay, M. A.; Diana, G. D.; Otto, M. J. *Science* **1986**, *233*, 1286.

8. Diana, G. D.; Oglesby, R. C.; Akullian, V.; Carabateas, P. M.; Cutcliffe, D.; Mallamo, J. P.; Otto, M. J.; McKinlay, M. A.; Maliski, E. G.; Michalec, S. J. *J. Med. Chem.* **1987**, *30*, 383.

9. Diana, G. D.; McKinlay, M. A.; Otto, M. J.; Akullian, V.; Oglesby, R. C. *J. Med. Chem.* **1985**, *28*, 1906.

10. Bailey, T. R.; Diana, G. D.; Kowalczyk, P. J.; Akullian, V.; Eissenstat, M. A.; Mallamo, J. P. *J. Med. Chem.* **1992**, *35*, 4628.

11. Guha-Biswas, M.; Holder, M.; Pettitt, B. M. *J. Med. Chem.* **1993**, *36*, 3489.

12. Massa, S.; Artico, M.; Mai, A.; Ragno, R.; Corelli, F.; Pani, A.; Marongiu, M. E.; Tramontano, E.; La Colla, P. *Bioorg. Med. Chem. Lett.* **1991**, *1*, 575.

13. Artico, M.; Corelli, F.; Massa, S.; Mai, A. Eur. Pat. Appl. EP 509 469, 1992; *Chem. Abstr.* **1993**, *118*, 124523x.

14. Massa, S.; Corelli, F.; Artico, M.; Mai, A.; Ragno, R.; De Montis, A.; Loi, A. G.; Corrias, S.; Marongiu, M. E.; La Colla, P. *J. Med. Chem.* **1995**, *38*, 803.

15. Mai, A.; Artico, M.; Massa, S.; Ragno, R.; De Montis, A.; Corrias, S.; Spiga, M. G.; La Colla, P. *Antiviral Chem. Chemother.* **1996**, *7*, 213.

16. Mai, A.; Massa, S.; Ragno, R.; Artico, M.; De Montis, A.; Loi, A. G.; Corrias, S.; Spiga, M. G.; La Colla, P. Proceedings of the 11th National Meeting of the Division of Medicinal Chemistry of the Italian Chemical Society, Bari (Italy), 2–5 Oct. 1994, Abstract P123.

17. Cramer, R. D.; DePriest, S. A.; Patterson, D. E.; Hecht, P. In *3D QSAR in Drug Design*; Kubinyi, H., Ed.; ESCOM: Leiden, 1993; pp 443–485.

18. Kim, K. H. *Quant. Struct.-Act. Relat.* **1995**, *14*, 8.

19. Steliou, K. MODEL (version 2.99) and BKMDL, Boston University, MA.

20. Cramer, R. D.; Patterson, D. E.; Bunce, J. D. *J. Am. Chem. Soc.* **1988**, *110*, 5959.

21. Tripos Associates, 1699 S. Hanley Road, Suite 303, St. Louis, MO 63144.

22. DePriest, S. A.; Mayer, D.; Naylor, C. B.; Marshall, G. R. *J. Am. Chem. Soc.* **1993**, *115*, 5372.

23. Stahle, L.; Wold, S. *J. Chemom.* **1987**, *1*, 185.

24. Wold, S.; Esbensen, K.; Geladi, P. *Chemometr. Intell. Lab. Sys.* **1987**, *2*, 37.

25. Cramer, R. D.; Bunce, G. D.; Patterson, D. E.; Frank, I. E. *Quant. Struct.-Act. Relat.* **1988**, *7*, 18.

26. Clark, M.; Cramer, R. D. *Quant. Struct.-Act. Relat.* **1993**, *12*, 137.

27. Badger, J.; Minor, I.; Kremer, M. J.; Oliveira, M. A.; Smith, T. J.; Griffith, J. P.; Guerin, D. M. A.; Krishnaswamy, S.; Luo, M.; Rossmann, M. G.; McKinlay, M. A.; Diana, G. D.; Dutko, F. J.; Fancher, M.; Rueckert, R. R.; Heinz, B. A. *Proc. Natl. Acad. Sci. U.S.A.* **1988**, *85*, 3304.

28. Diana, G. D.; Otto, M. J.; Treasuriwala, A. M.; McKinlay, M. A.; Oglesby, R. C.; Maliski, E. G.; Rossmann, M. G.; Smith, T. J. *J. Med. Chem.* **1988**, *31*, 540.

29. Podlogar, B. L.; Farr, R. A.; Friedrich, D.; Tarnus, C.; Huber, E. W.; Cregge, R. J.; Schirlin, D. *J. Med. Chem.* **1994**, *37*, 3684.

30. It is interesting to remark that the interaction energy of the complexes is essentially steric energy. This is in agreement with both our CoMFA results and Diana's QSAR studies, in which the antiviral activity of the compounds resulted to correlate quite well with their molecular weight, taken as a descriptor of steric bulkiness.

31. El Tayar, N.; van de Waterbeemd, H.; Testa, B. *J. Chromatogr.* **1985**, *320*, 293.

(*Received in U.S.A.* 18 *March* 1996; *accepted* 28 *June* 1996)